Acta Oceanol. Sin., 2017, Vol. 36, No. 5, P. 99–104
DOI: 10.1007/s13131-017-1064-5
http://www.hyxb.org.cn
E-mail: hyxbe@263.net

A new electroplated Ir/Ir(OH)$_x$ pH electrode and its application in the coastal areas of Newport Harbor, California

ZHANG Xiao[1], YE Ying[1], KAN Yating[1], HUANG Yuanfeng[1], JIA Jianjun[1], ZHAO Yue[1], CHEN Chen-Tung Arthur[1, 2], QIN Huawei[3]*

[1] Ocean College, Zhejiang University, Zhoushan 316000, China

[2] Institute of Marine Geology and Chemistry, National Sun Yat-sen University, Kaohsiung 80424, Taiwan, China

[3] School of Mechanical Engineering, Hangzhou Dianzi University, Hangzhou 310018, China

Received 7 March 2016; accepted 27 July 2016

Abstract

Resulting from the rising levels of atmospheric carbon, ocean acidification has become a global problem. It has significant impacts on the development, survival, growth and physiology of marine organisms. Therefore, a high-precision sensor is urgently needed to measure the pH of sea-water. Iridium wire with a diameter of 0.25 mm is used as the substrate, and an Ir/Ir(OH)$_x$ pH electrode is prepared by a one-step electrochemical method in a LiOH solution at the room temperature. A scanning electron microscope (SEM) observation reveals that it is coated with nanoscale particles. In laboratory tests, the electrode exhibits a very promising pH response, with an ideal Nernst slope (56.14–59.52), fast response, good stability and long life-span in tested pH buffer solutions. For a sea trial, four pH electrodes and one Ag/AgCl reference electrode are integrated with a self-made chemical sensor, and a profile detection of nearly 70 m is implemented near Newport Harbor, California on August 3, 2015. The results reflect that the pH value measured by the sensor is very close to the data given by Sea-Bird 911 plus CTD, with a difference value ranging from 0.000 075 to 0.064 719. And the sensor shows a better data matching degree in 0–40 m water depth. In addition, the high precision and accuracy of the sensor make it possible to use in the ocean observation field.

Key words: Ir/Ir(OH)$_x$ electrode, pH value, electroplating, Newport Harbor, California

Citation: Zhang Xiao, Ye Ying, Kan Yating, Huang Yuanfeng, Jia Jianjun, Zhao Yue, Chen Chen-Tung Arthur, Qin Huawei. 2017. A new electroplated Ir/Ir(OH)$_x$ pH electrode and its application in the coastal areas of Newport Harbor, California. Acta Oceanologica Sinica, 36(5): 99–104, doi: 10.1007/s13131-017-1064-5

1 Introduction

The concentration of global CO_2 has increased about 1×10^{-4} (36%) over the latest 250 a, from a range of 180×10^{-6} to 285×10^{-6} in the pre-industrial era (Feely et al., 2004; He et al., 2014) to 391×10^{-6} in 2014 (Wang et al., 2012). The growth rate of the particle pressure of carbon dioxide (p_{CO_2}) in the atmosphere was about 0.5% each year (He et al., 2014), threatening a continually rising p_{CO_2} level in sea water. It also results in a decline of pH values in sea water, which will make the water acidic.

To enable improved investigation of this global problem of ocean acidification, an accurate and economical sensor is badly needed to measure the pH of sea water. A properly-designed sensor could not only monitor ocean acidification effect on marine organisms and ecosystems, but also play an important role in the development of the marine services, data, information, prediction and global industry (Das and Mangwani, 2015).

In situations where glass electrodes are unsuitable or inconvenient at high temperatures or on a microscale (Cheng et al., 2011; Chen et al., 2007), metal oxide all-solid-state electrodes have shown potential to substitute for glass pH electrodes (Yao et al., 2001). Various solid-state metal oxides have been investigated for pH electrodes, such as TiO_2 (Zhao et al., 2010), RuO_2 (Maurya et al., 2013), PtO (Kreider et al., 1995), Ta_2O_5 (Gimmel et al., 1989), WO_3 (Yamamoto et al., 2003; Xu and Zhang, 2010), and IrO_x (Kim and Yang, 2014). Among these oxides, IrO_x and RuO_2 were the most prospective electrode materials based on the indication of pH sensitivity, working pH range, ion and redox interferences, and hysteresis (Fog and Buck, 1984).

Several preparation methods for the IrO_x (hydrous and anhydrous) electrodes have been reported, including sputtered coating (Tarlov et al., 1990; Kuo et al., 2014), melting method (Ardizzone et al., 1981; Huang et al., 2011), electrochemical growth (Burke and Whelan, 1984; Olthuis et al., 1990), etc. The first two methods resulted in dense and poorly hydrated oxides which are referred to as anhydrous. The thickness and structure of the IrO_x film were uneven and not easy to control at the high temperature. And when the electrode got cold, the film would be easily peeled off from the metal substrate as a result of different shrinkage rates of these two layers (Pan and Seyfried Jr, 2008; Han et al., 2009). The damageable characteristic made this kind of pH electrode unable to achieve the anticipated effects in measurements.

A considerable amount of research has focused on the electrochemical growth, for its deposition uniformity and controllability. Using cyclic voltammetry, an anodic iridium oxide film

Foundation item: The Key Laboratory Project of State Oceanic Administration for Marine Ecosystem and Biogeochemistry of China under contract No. 529101-X21601; the Foundation from Wendy Schmidt Ocean Health XPRIZE and the Southern California Coastal Water Research Project.

*Corresponding author, E-mail: qinhw@hdu.edu.cn

could be deposited in acidic solutions (Burke and Whelan, 1984), while it was a hydrous iridium oxide film in alkaline solutions (Baur and Spaine, 1998; Steegstra and Ahlberg, 2012). However, complicated preparation is an un-resolved problem.

An easily-operated preparation method is introduced in this work. LiOH solution was used as the electrolyte, to fabricate an $Ir/Ir(OH)_x$ electrode. Owing to the room temperature fabrication, this film has strong adhesion to the metal substrate. Furthermore, the thickness and structure could be easily controlled by electrochemical parameters.

The electrodes were mounted to an ocean acidification sensor. This was used for measuring the pH value of the sea water near Newport Harbor, California. Fabrication procedure, data processing, surface characterization and calibration results are summed up in this paper.

2 Experiments

2.1 *Ir/Ir(OH)$_x$ pH electrode preparation and laboratory test*

2.1.1 *Chemical reagents and apparatus*

Iridium wire (99.9%, 0.25 mm in diameter) was purchased from Johnson Matthey Company, USA. Silver wire (99.9%, 0.6 mm in diameter) was obtained from the Precious Materials Company, Changzhou, China. LiOH (99.9%) and NaCl (99.8%) were from Sigma-Aldrich. pH standard buffer solutions of 4.00, 6.86 and 9.18 were prepared with potassium hydrogen phthalate (KHP, obtained from Sinopharm Chemical Reagent) which was dissolved 3.5% NaCl to simulate the salinity of sea water.

All electrochemical studies were made by CHI760D electrochemical workstation (Chenhua Company, Shanghai, China). A scanning electron microscopy (SEM; SU-70, Hitachi, Japan) was used to observe the surface structure of the electrode. Experiments were all performed at an ambient temperature [(25±1)°C].

2.1.2 *Preparation of Iridium wire*

Iridium wires of about 2–3 cm in length were ultrasonically cleaned in 5 mol/dm^3 HCl and de-ionized water alternately for 10 min. To attach the electrode to the detector part on the chemical sensor, gas welding was then used to connect the Iridium wire with a silver wire.

2.1.3 *Ir(OH)$_x$ film coating*

The cyclic voltammetry (CV) method of the CHI760D electrochemical workstation was used to electroplate the $Ir(OH)_x$ film on the Iridium wire in 5% LiOH solution, scanning from 0 to 0.7 V at a rate of 50 mV/s for three cycles. In the three-electrode system, the working electrode was the Iridium wire, the reference electrode was a commercial Ag/AgCl, Cl^- electrode, and the auxiliary electrode was a Pt electrode.

Then the product was rinsed with deionized water and ethanol successively, and naturally dried in air. Finally, the electrode was immersed in 3.5% NaCl solution for at least 4 h for the purpose of improving the activation.

2.2 *Sensor assembly*

A schematic picture of the ocean acidification sensor is illustrated in Fig. 1a. It has a cylindrical shape with a length of 230 mm and a width of 73 mm (Ding et al., 2015). Titanium alloy was used to fabricate the sensor body because of its excellent high specific strength and corrosion resistance (Huang et al., 2005). The sensor was comprised of several parts: a temperature sensor, communication port and detector part outside and a circuit board for data recording and a battery inside.

Four pH electrodes and an Ag/AgCl reference electrode were all fixed on the detector part (Fig. 1b). The Ag/AgCl reference electrode was prepared by a melting method (Xie and Liu, 1998). Each electrode had a corresponding characteristic position, centered the reference electrode, to dampen the distance effects. The exposed metal rods of the probe were wrapped in two shrinkable tubes and an epoxy resin adhesive layer in sequence. In practical sea trials, a pure copper cap was screwed on the detector part, to get rid of the adhesion of sea creatures to the electrode.

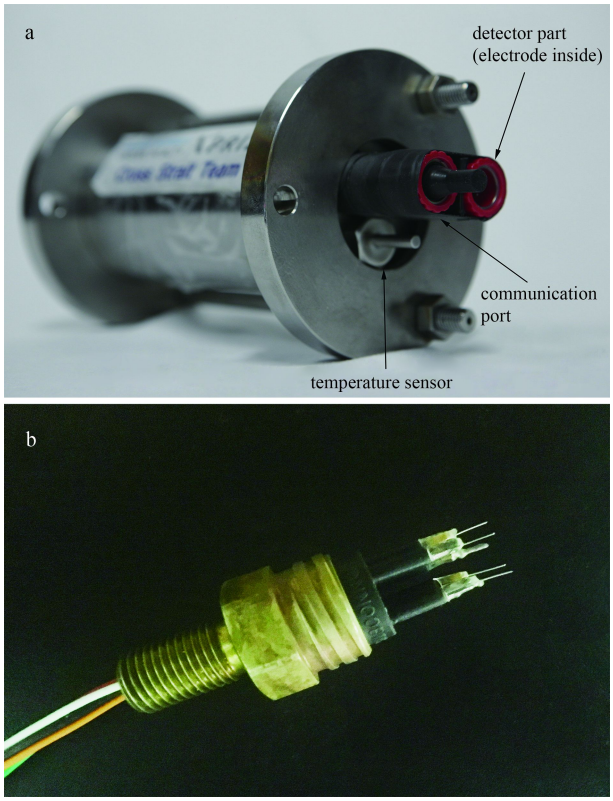

Fig. 1. The appearance of the sensor (a) and the image of the detector component (b).

3 Sea trial

Calibrations were the first step to obtain standard data. Electrodes were run in Tris (*pH*=8.093 6) (Bates and Erickson, 1986; Dickson, 1993a, b; Whitfield et al., 1985) and Dickson sea water (*pH*=7.87 60, obtained from University of California, San Diego) for 10 min, respectively. The data processing of the two calibrations will be discussed in Section 4.2.

We started from Newport Harbor of southwest California on August 3, 2015. The sea trial was conducted in the sea area near Newport Beach (Fig. 2). Newport Beach's climate is greatly moderated by the Pacific Ocean with warm winter temperatures and cooling summer temperatures. Surface water near the beach had a maximum temperature of 24°C and a minimum temperature of 19°C (McLaughlin et al., 2007).

On the threshold of the sea trial, the electrode probes were wrapped in a semi-open cell, to slow down the water scouring. The sensor was strapped to a Sea-Bird 911 plus CTD. Then the two devices were carefully timed and both tuned to a sampling frequency of 8 Hz. When these preparations were completed, a

profile detection was implemented at 33°33'28.8''N, 117°52'30.0''W (Fig. 2), by casting CTD down to near 70 m deep, and pulling it up to the deck after a while. The time for calibration, entering the sea, reaching the sea bottom and returning to the sea surface has been manually recorded in Table 1.

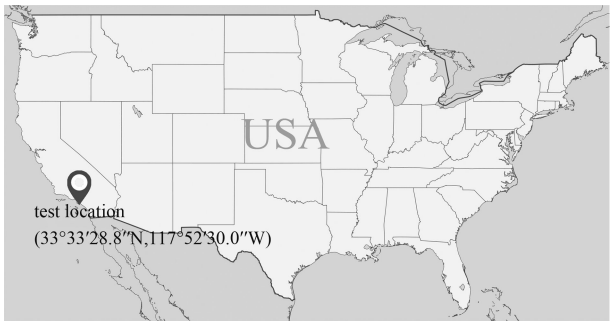

Fig. 2. Test area, located at 33°33′28.8″N, 117°52′30.0″W, near Newport Harbor, California, USA.

Table 1. Working points of the sensor

Point	Sensor state	Start (local time)	End (local time)
1	woken up	08:38:21	
2	in Dickson sea-water	08:45:12	08:46:12
3	in Tris solution	08:47:53	08:57:53
4	entered the sea	09:22:15	
5	reached sea-bottom	09:23:38	
6	back to sea surface	09:25:52	
8	in sleeping state	09:30:33	

Note: The date is on August 3, 2015; the sensor is OE64; the latitude is 33°33′28.8″N and the longitude is 117°52′30.0″W.

4 Data processing

4.1 *Data organization and primary correction*

Data batched from the sensor were placed in an Excel spreadsheet and was named as OE64-August 3, 2015.

In the raw data table, each line corresponds to one measured data point. The header lists the name of data measured by the sensor, which contain time, counter, potential values (U_1) and temperature (T).

To correct the signal intensity against equipment error, one more column was added after U_1 and named as U_2:

$$U_2 = (U_1 - B_1)/A_1, \tag{1}$$

where A_1 and B_1 are the slope and intercept of correcting equation. For OE64, A_1=0.999 8, B_1=0.228 6.

After organization as above, part of the data in the file was listed in Table 2.

4.2 *Data processing in standard solutions*

Data at time of Point 2 (in Dickson sea water) and Point 3 (in Tris solution) in Table 1 were pasted into a new sheet named data-2 in Sheet 2.

The drifting curve and its calibration in Dickson sea water are shown in Fig. 3. The first relative minimum (FRM) is regarded as a reference point, and the one more column (U_2) is corrected to a stable value (U_2') with a linear fit.

The calibration in Tris solution works in the same way.

Table 2. Lay-out of Sheet 1 (data-1) in the file

Time	Counter	U_1/mV	U_2/mV	T/°C
09:22:15.000	1	−129.580	−129.835	22.093 5
09:22:15.125	2	−129.540	−129.795	22.108 7
09:22:15.250	3	−129.540	−129.795	22.114 4
09:22:15.375	4	−129.540	−129.795	22.111 9
09:22:15.500	5	−129.500	−129.755	22.104 6
09:22:15.625	6	−129.430	−129.685	22.062 3
09:22:15.750	7	−129.470	−129.725	22.076 5
09:22:15.875	8	−129.430	−129.685	22.054 3
09:22:16.000	9	−129.430	−129.685	22.022 5
09:22:16.125	10	−129.400	−129.655	22.004 4
09:22:16.250	11	−129.400	−129.655	21.977 2
09:22:16.375	12	−129.400	−129.655	21.970 6
09:22:16.500	13	−129.400	−129.655	21.984 1
09:22:16.625	14	−129.360	−129.615	21.971 2
09:22:16.750	15	−129.400	−129.655	21.966 0
09:22:16.875	16	−129.400	−129.655	22.022 2

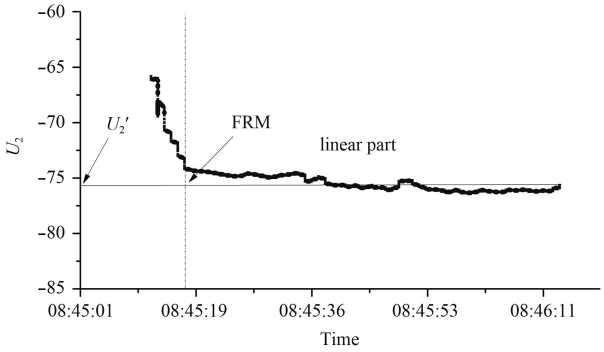

Fig. 3. Dickson sea water is measured for 1 min, at 8 Hz frequency. The drifting curve was divided into two parts by the first relative minimum (FRM): non-linear part on the left, and linear part on the right. The intercept of the linear part on the *y* axis is the corrected value (U_2').

4.3 *mV-pH conversion standard building*

In Sheet 3, with known pH value of Dickson (pH=7.876 0) and Tris standard solutions (pH=8.093 6), the stable value (U_2') in both Dickson and Tris should be corrected by a temperature coefficient:

$$U_{25} = A_2(25 - T) + U_2', \tag{2}$$

where U_{25} is the signal intensity at 25°C, T is the measured temperature; and A_2 is the measured temperature coefficient for certain solutions, which unit is mV/°C. For Dickson, A_2=−0.015 1, and for Tris, A_2=−0.009 4.

Then a U-pH mapping relationship was built based on the U_{25} and pH_{25} in two standard solutions, and the slope (A_3) and the intercept (B_3) of this linear relationship could be calculated as follows:

$$pH_{25} = A_3 \cdot U_{25} + B_3. \tag{3}$$

4.4 *pH value calculation*

Based on the U-pH relationship, the measured profile data in Sheet 1 could be calculated as

$$pH_{in\ situ} = (U_2 - B_3)/A_3, \quad (4)$$

where $pH_{in\ situ}$ is the *pH* value at the *in situ* temperature.

And the pH value at 25°C was calculated as follows:

$$pH_{25}=pH_{in\ situ} - A_2(25 - T), \quad (5)$$

where A_2 is the temperature coefficient (–0.015 1 mV/°C) of sea water.

The final calculated results will be discussed in Section 5.3.

5 Results and discussion

5.1 *SEM observation of pH electrode*

The SEM photographs of an Iridium wire and an Iridium wire coated with the $Ir(OH)_x$ film are displayed in Figs 4a and b. By comparison, it is found that the $Ir(OH)_x$ film formed by *in situ* electrochemical reaction was dense and compact. The electrode surface was covered by quite small particles with a diameter of 50–200 nm as shown in the photograph after 50 000 magnification. This thin film with nano-sized particles is quite possibly the major reason for the good performance of the electrode as revealed in the next section.

5.2 *Performance test of pH electrode*

5.2.1 *Potential pH response*

Potentiometric pH measurements were carried out by registering an open circuit potential of an $Ir/Ir(OH)_x$ pH electrode against an Ag/AgCl reference electrode (Prats-Alfonso et al., 2013). Figure 5 shows the linear fitting result in pH buffer solutions of 4.00, 6.86 and 9.18. The slopes between the response potential and pH were 56.14–59.52, close to the values predicted by the Nernst Equation (Huang et al., 2015). The correlation coefficients (R^2) of these linear regressions were between 0.999 15 and 0.999 99.

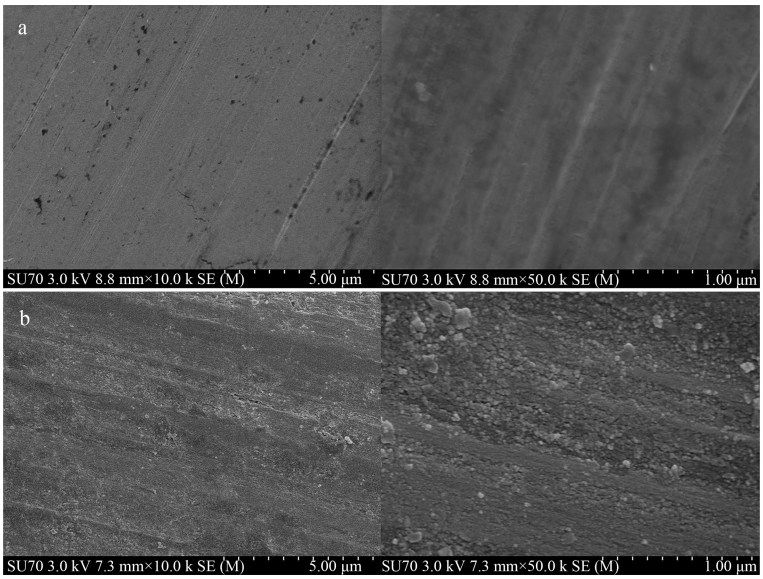

Fig. 4. The SEM photographs of Iridium wire (a) and Iridium wire coated with $Ir(OH)_x$ film (b) after 10 000 and 50 000 magnification.

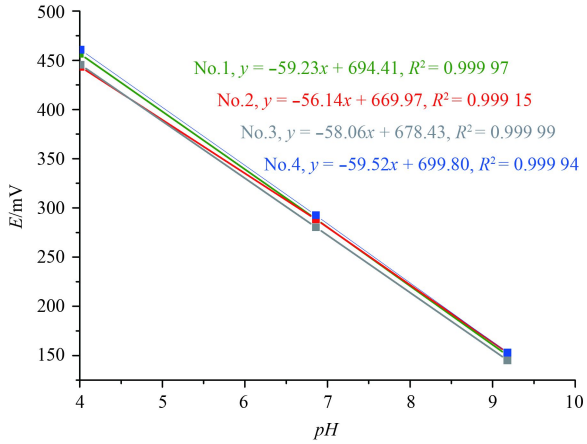

Fig. 5. The calibration curves of the $Ir/Ir(OH)_x$ pH electrode.

5.2.2 *Response time and stability*

Figure 6 shows the calibration process of four pH electrodes and an Ag/AgCl reference electrode in pH buffer solutions. The potential reading was taken for 200 s. Constant signals were obtained promptly after the electrode entered the solution. It took only 5 s to achieve a stable signal as shown in Fig. 3. Compared with the response time of 15 s as reported in the literature (Da Silva et al., 2008), the response of our pH electrodes was faster. In each calibration period of 200 s, the electrode had no obvious signal decay, nor response failure. After enlarging the calibration curve of *pH*=6.86 in Fig. 6, signals remained extremely stable, with an absolute potential drift of 0.4–2.9 mV and a potential standard deviation of 0.06–0.92 mV.

5.2.3 *Accuracy*

Accuracy is a required property in pH measurements for practical applications. Dickson sea water was taken to validate the correctness of the electrode. After calibrations in pH buffer solutions of 6.86 and 9.18, pH of Dickson sea water measured by the $Ir/Ir(OH)_x$ electrode was 7.875 1, which was in excellent agreement with the actual value (*pH*=7.876 0). Moreover, the accuracy of the electrode was further confirmed in sea trial results of Section 5.3.

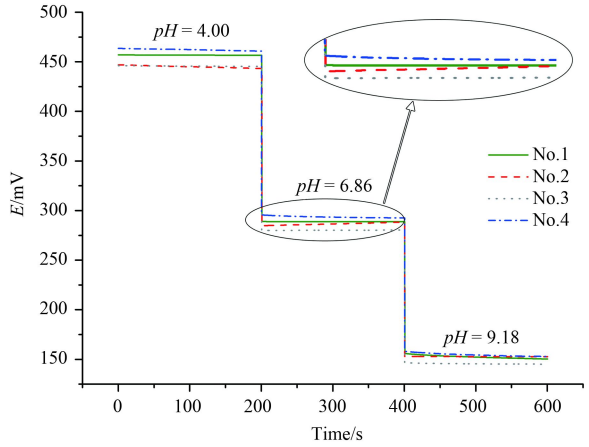

Fig. 6. Calibration process of four pH electrodes in pH buffer solutions.

5.2.4 *Life-span*

To evaluate the long-term stability of the pH electrode, calibration experiments were performed continuously for 137 days. The Nernst slopes (k) and correlation coefficients (R^2) are shown in Table 3. Good pH responses were maintained during the whole period of the life-span test, with Nernst slopes of 57.83–59.80. It indicates that the pH electrode will likely be used for more than 5 months.

Table 3. The Nernst responses of the Ir/Ir(OH)$_x$ pH electrode continuously calibrated for 137 days

Date	k	R^2	Date	k	R^2
2014-11-14	59.77	1.000 00	2014-12-26	59.12	0.997 68
2014-11-20	59.80	0.999 97	2015-01-02	58.02	0.999 89
2014-11-28	57.93	0.999 95	2015-01-15	58.01	0.999 17
2014-12-05	58.76	0.999 93	2015-02-22	57.83	0.999 63
2014-12-12	58.92	0.999 19	2015-03-10	57.87	0.999 61
2014-12-19	59.33	0.999 93	2015-03-31	58.27	0.999 83

5.3 *pH value test results in the sea trial*

The results comparison is shown in Table 4 (the average for every 10 s is shown because of the enormous amount of data). It can be seen that the results of our ocean acidification sensor (OAS) are very close to the data given by Sea-Bird 911 plus CTD (OCSD). The differences in pH values are quite small, and range from 0.000 075 to 0.064 719 pH units. It indicates our OAS can achieve the goal of high precision. Meanwhile, the relationship between the water depth and pH value of these two sensors is clearly shown in Fig. 7. The right-to-left curve is the entire cast process. The red and blue curves represent the results of OAS and OCSD, respectively. The development data trend of 0–40 m water depth demonstrates that the OAS is better than the OCSD, with closer data matching in the two phases.

6 Conclusions

A novel all-solid-state Ir/Ir(OH)$_x$ pH electrode was fabricated by a one-step cyclic voltammetry method. Prepared at the room temperature, the film combined tightly with the Iridium substrate. The SEM photographs indicated that the film was dense and compact. In the performance test, the pH electrode was characterized by ideal Nernst response (56.14–59.52 mV/pH), fast response, good stability and long life-span in pH buffer solutions.

On the basis of the advantage of its small size and easy integration, four Ir/Ir(OH)$_x$ pH electrodes and an Ag/AgCl reference electrode were integrated with a chemical sensor. It was used to measure pH values in a California sea area on August 3, 2015, along with the Sea-Bird 911 plus CTD. Processed by our own reliable method, pH values in the entire profile were calculated in Microsoft Excel. The comparison result shows a close relation between these two instruments, with a difference pH value ranging from 0.000 075 to 0.064 719. And the data matching degree of our ocean acidification sensor at 0–40 m water depth was better than that of the Sea-Bird. Therefore, high precision and accuracy are evident for our sensor.

With these features and advantages, the ocean acidification sensor with integrated Ir/Ir(OH)$_x$ pH electrodes will have broad application prospects in the field of global ocean observation.

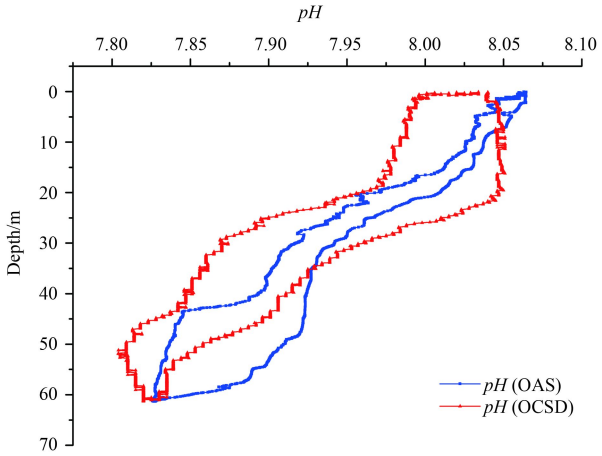

Fig. 7. The relationship between the water depth and pH value of two measuring apparatuses. Right to left is the cast direction. Measured pH value by the OAS was quite similar to that measured by the OCSD, or even more accurate.

Table 4. pH data comparison between the OAS and the OCSD during the whole cast (average every 10 s)

Local time	Depth/m	pH(OAS)	pH(OCSD)	Local time	Depth/m	pH(OAS)	pH(OCSD)
09:22:20	2.259 85	8.060 252	8.043 200	09:24:00	49.850 50	7.837 876	7.811 913
09:22:30	9.374 80	8.040 793	8.047 463	09:24:10	42.176 16	7.870 407	7.841 837
09:22:40	17.539 84	8.016 856	8.047 150	09:24:20	34.574 01	7.903 677	7.859 138
09:22:50	25.776 43	7.963 112	8.002 088	09:24:30	26.741 41	7.931 623	7.892 238
09:23:00	33.984 45	7.930 711	7.935 787	09:24:40	18.897 04	7.980 512	7.962 062
09:23:10	42.231 69	7.923 005	7.905 175	09:24:50	11.377 56	8.023 358	7.981 650
09:23:20	50.293 60	7.909 176	7.860 100	09:25:00	4.329 388	8.039 04	7.990 713
09:23:30	58.104 53	7.868 933	7.833 813	09:25:10	1.256 500	8.055 551	7.997 325
09:23:40	60.887 73	7.830 575	7.824 500	09:25:20	0.516 350	8.059 633	8.006 150
09:23:50	57.182 21	7.829 722	7.815 375				

References

Ardizzone S, Carugati A, Trasatti S. 1981. Properties of thermally prepared iridium dioxide electrodes. J Electroanal Chem Interfacial Electrochem, 126(1–3): 287–292

Bates R G, Erickson W P. 1986. Thermodynamics of the dissociation of 2-aminopyridinium ion in synthetic seawater and a standard for pH in marine systems. J Solution Chem, 15(11): 891–901

Baur J E, Spaine T W. 1998. Electrochemical deposition of iridium (IV) oxide from alkaline solutions of iridium(III) oxide. J Electroanal Chem, 443(2): 208–216

Burke L D, Whelan D P. 1984. A voltammetric investigation of the charge storage reactions of hydrous iridium oxide layers. J Electroanal Chem Interfacial Electrochem, 162(1–2): 121–141

Chen Dongchu, Li Wenfang, Huang Jinying. 2007. Preparation of a tungsten oxide pH electrochemical sensor based on solid Ag/AgCl reference electrode. Chin J Sens Actuators, 20(7): 1483–1487

Cheng Changming, Tian Xianqing, Guo Yong, et al. 2011. Large enhancement of sensitivity and a wider working range of glass pH electrode with amperometric and potentiometric responses. Electrochim Acta, 56(27): 9883–9886

Da Silva G M, Lemos S G, Pocrifka L A, et al. 2008. Development of low-cost metal oxide pH electrodes based on the polymeric precursor method. Anal Chim Acta, 616(1): 36–41

Das S, Mangwani N. 2015. Ocean acidification and marine microorganisms: responses and consequences. Oceanologia, 57(4): 349–361

Dickson A G. 1993a. pH buffers for sea water media based on the total hydrogen ion concentration scale. Deep-Sea Res: Part I. Oceanogr Res Pap, 40(1): 107–118

Dickson A G. 1993b. The measurement of sea water pH. Mar Chem, 44(2–4): 131–142

Ding Qian, Pan Yiwen, Huang Yuanfeng, et al. 2015. The optimization of Ag/Ag_2S electrode using carrier electroplating of nano silver particles and its preliminary application to offshore Kueishan Tao, Taiwan. Cont Shelf Res, 111: 262–267

Feely R A, Sabine C L, Lee K, et al. 2004. Impact of anthropogenic CO_2 on the $CaCO_3$ system in the oceans. Science, 305(5682): 362–366

Fog A, Buck R P. 1984. Electronic semiconducting oxides as pH sensors. Sens Actuators, 5(2): 137–146

Gimmel P, Gompf B, Schmeisser D, et al. 1989. Ta_2O_5-gates of pH-sensitive devices: comparative spectroscopic and electrical studies. Sens Actuators, 17(1–2): 195–202

Han Chenhua, Pan Yiwen, Ye Ying. 2009. CO_2 microelectrode based on Zn-Al-LDH-ion carrier and its characterization. J Trop Oceanogr (in Chinese), 28(4): 35–41

He Shichang, Zhang Yuanhui, Chen Liqi, et al. 2014. Advances in the studies of ocean acidification. Mar Sci (in Chinese), 38(6): 85–93

Huang Wending, Cao H, Deb S, et al. 2011. A flexible pH sensor based on the iridium oxide sensing film. Sens Actuators: A. Phys, 169(1): 1–11

Huang Yuanfeng, Li Jun, Yin Tianya, et al. 2015. A novel all-solid-state ammonium electrode with polyaniline and copolymer of aniline/2, 5-dimethoxyaniline as transducers. J Electroanal Chem, 741: 87–92

Huang Xiaoyan, Liu Bo, Li Xue. 2005. Applications of titanium alloys in warship building. Southern Met (in Chinese), (6): 10–11, 33

Kim T Y, Yang S. 2014. Fabrication method and characterization of electrodeposited and heat-treated iridium oxide films for pH sensing. Sens Actuators: B. Chem, 196: 31–38

Kreider K G, Tarlov M J, Cline J P. 1995. Sputtered thin-film pH electrodes of platinum, palladium, ruthenium, and iridium oxides. Sens Actuators: B. Chem, 28(3): 167–172

Kuo Limin, Chou Y C, Chen Kuanneng, et al. 2014. A precise pH microsensor using RF-sputtering IrO_2 and Ta_2O_5 films on Pt-electrode. Sens Actuators: B. Chem, 193: 687–691

Maurya D K, Sardarinejad A, Alameh K. 2013. High-sensitivity pH sensor employing a sub-micron ruthenium oxide thin-film in conjunction with a thick reference electrode. Sens Actuators: A. Phys, 203: 300–303

McLaughlin K, Ahn J H, Litton R M, et al. 2007. Use of salinity mixing models to estimate the contribution of creek water fecal indicator bacteria to an estuarine environment: Newport Bay, California. Water Res, 41(16): 3595–3604

Olthuis W, Robben M A M, Bergveld P, et al. 1990. pH sensor properties of electrochemically grown iridium oxide. Sens Actuators: B. Chem, 2(4): 247–256

Pan Yiwen, Seyfried W E Jr. 2008. Experimental and theoretical constraints on pH measurements with an iridium oxide electrode in aqueous fluids from 25 to 175°C and 25 MPa. J Solution Chem, 37(8): 1051–1062

Prats-Alfonso E, Abad L, Casañ-Pastor N, et al. 2013. Iridium oxide pH sensor for biomedical applications. Case urea-urease in real urine samples. Biosens Bioelectron, 39(1): 163–169

Steegstra P, Ahlberg E. 2012. Influence of oxidation state on the pH dependence of hydrous iridium oxide films. Electrochim Acta, 76: 26–33

Tarlov M J, Semancik S, Kreider K G. 1990. Mechanistic and response studies of iridium oxide pH sensors. Sens Actuators: B. Chem, 1(1–6): 293–297

Wang Siru, Yin Kedong, Cai Weijun, et al. 2012. Advances in studies of ecological effects of ocean acidification. Acta Ecol Sinica (in Chinese), 32(18): 5859–5869

Whitfield M, Butler R A, Covington A K. 1985. The determination of pH in estuarine waters I. Definition of pH scales and the selection of buffers. Oceanol Acta, 8(4): 423–432

Xie Zhong, Liu Yexiang. 1998. Reference electrode for electrochemical studies in fused chloride. Chin J Nonferrous Met (in Chinese), 8(4): 668–672

Xu Bin, Zhang Weide. 2010. Modification of vertically aligned carbon nanotubes with RuO_2 for a solid-state pH sensor. Electrochim Acta, 55(8): 2859–2864

Yamamoto K, Shi Guoyue, Zhou Tianshu, et al. 2003. Solid-state pH ultramicrosensor based on a tungstic oxide film fabricated on a tungsten nanoelectrode and its application to the study of endothelial cells. Anal Chim Acta, 480(1): 109–117

Yao Sheng, Wang Min, Madou M. 2001. A pH electrode based on melt-oxidized iridium oxide. J Electrochem Soc, 148(4): H29-H36

Zhao Rongrong, Xu Meizhu, Wang Jian, et al. 2010. A pH sensor based on the TiO_2 nanotube array modified Ti electrode. Electrochim Acta, 55(20): 5647–5651